ACS APPLIED MATERIALS & INTERFACES

Research Article

www.acsami.org

# Fabrication of Graphene Embedded $LiFePO_4$ Using a Catalyst Assisted Self Assembly Method as a Cathode Material for High Power Lithium-Ion Batteries

WonKeun Kim,[†] WonHee Ryu,[†] DongWook Han,[†] SungJin Lim,[†] JiYong Eom,*[,‡] and HyukSang Kwon*[,†]

[†]Department of Materials Science and Engineering, Korea Advanced Institute of Science and Technology, 291 Daehak-ro, Yuseong-gu, Daejeon 305-701, Republic of Korea

[‡]Clean & Energy Materials R&D Center, Automotive Materials Convergence & System R&D Division, Korea Automotive Technology Institute, 303 Pungse-ro, Pungse-myeon, Dongnam-gu, Cheonan-si, Chungnam 330-912, Republic of Korea

Supporting Information

**ABSTRACT:** We have designed a unique microstructure of graphene embedded $LiFePO_4$ by a catalyst assisted self assembly method as a cathode material for high power lithium-ion batteries. The stable amide bonds between $LiFePO_4$ and graphene were formed by the catalyst assisted self assembly. High conductive graphene provides a fast electron transfer path, and many pores inside the structure facilitate the lithium-ion diffusion. The graphene embedded $LiFePO_4$ fabricated by the novel method shows enhanced cycling performance and rate-capability compared with that of carbon coated $LiFePO_4$ as a cathode material for high power lithium-ion batteries.

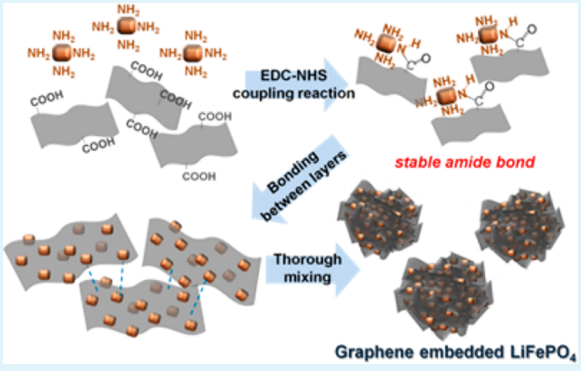


**KEYWORDS:** *$LiFePO_4$, graphene, catalyst assisted self assembly, cathode, lithium-ion battery*

## 1. INTRODUCTION

$LiFePO_4$ with an ordered olivine structure has received much attention as the most promising cathode material in large-sized lithium-ion batteries (LIBs) for electric vehicle (EV) and energy storage system (ESS) applications, due primarily to its advantageous material properties, such as high theoretical capacity (170 mA h $g^{-1}$), excellent structural stability, good cycling stability, low cost, and non-toxicity.[1−4] However, the pristine $LiFePO_4$ has the disadvantage of poor rate performance because of its low electrical conductivity ($\sim 10^{-1}$ S $cm^{-1}$) and Li-ion diffusivity ($\sim 10^{-14}$ $cm^2$ $s^{-1}$).[2−6] Recently, many approaches to improve the rate performance of $LiFePO_4$ have been studied through carbon nanotube (CNT) or graphene modification simultaneously with nano-sized $LiFePO_4$.[7−11]

In particular, intensive research on anode/cathode nanomaterials modified by graphene, including $LiFePO_4$, has been done due to its superior electrical conductivity, large surface area (2630 $m^2$ $g^{-1}$), and high thermal and chemical stability.[12−18] J. H. Ha et. al. reported chemically activated graphene encapsulated $LiFePO_4$ composites and their improved electrochemical performances.[19] However, the nano-sized particles of $LiFePO_4$ with high contents of graphene of about 10 wt % led to a decrease in the gravimetric/volumetric energy density because the tap density of a $LiFePO_4$ electrode decreases as the $LiFePO_4$ particle size reduces to the nanoscale and the amount of bulky conducting carbons increases to secure the electrical contact between the $LiFePO_4$ nanoparticles.[4,20,21] Therefore, it is very important to develop high performance $LiFePO_4$ modified by graphenes with micro-sized particles and low contents of graphenes.

Herein, we report a novel method for the fabrication of micro-sized and porous graphene embedded $LiFePO_4$ by 3D-assembly of $LiFePO_4$ primary nanoparticles with graphene sheets using stable amide bonds between them induced by catalyst. As expected, the micro-sized and porous graphene embedded $LiFePO_4$ exhibits better high rate cycling performance than that of the nano-sized $LiFePO_4$ coated with carbon.

## 2. EXPERIMENTAL SECTION

**2.1. Material Preparation and Characterization.** The $LiFePO_4$ (LFP) nanoparticles were synthesized by a hydrothermal process. The synthesized LFP was coated with carbon by the sucrose mixing method, denoted as CLFP. To fabricate the graphene embedded LFP, at first, a surface treatment of LFP with aminopropyl-trimethoxysilane (APTMS) was done by reflux to attach amine groups on the surface for 2 h. At the second step, the graphene oxide solution consisted of 10 mg of graphene oxide in 200 mL of deionized (DI) water, prepared

Received: November 26, 2013
Accepted: March 12, 2014
Published: March 12, 2014

   dx.doi.org/10.1021/am405335k | ACS Appl. Mater. Interfaces 2014, 6, 4731−4736

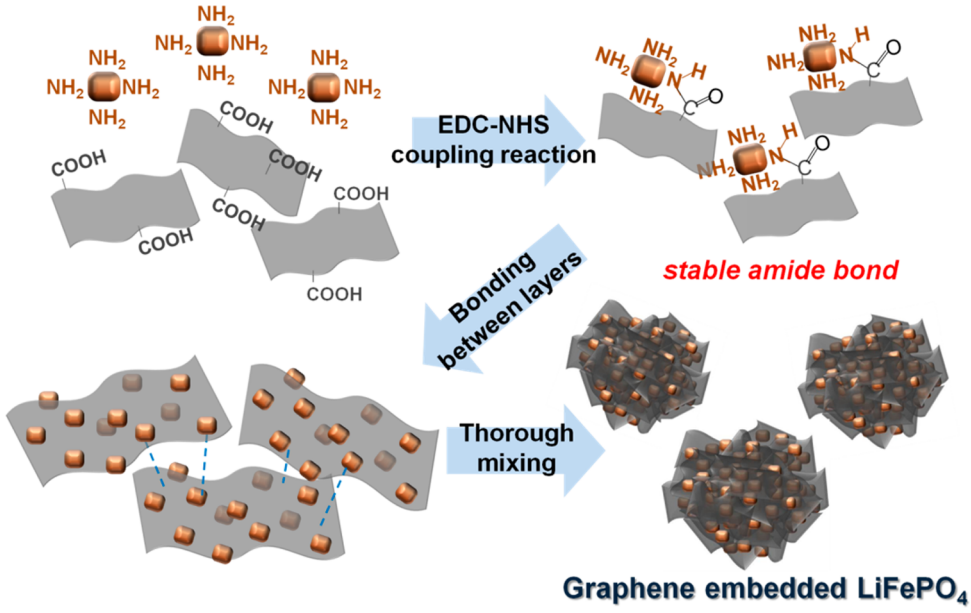


**Figure 1.** Schematic illustration of the catalyst assisted assembly method for fabrication of the graphene embedded $LiFePO_4$.

with the addition of 1-ethyl-3-(3-dimethylaminopropyl)carbodiimide (EDC)/*N*-hydroxysuccinimide (NHS) catalyst while the pH of the solution was adjusted to 4−6. Then, the surface treated LFP was dispersed into the graphene oxide solution and stirred for 1 h. Finally, 10 mL of hydrazine (35 wt %) was added to the mixture solution to reduce the graphene oxide, and the final solution was washed and filtered several times. The resultant powder was named graphene embedded LFP, denoted as GLFP.

The morphology of the pristine LFP, CLFP, and GLFP was characterized by scanning electron microscopy (SEM, Philips, XL 30 SFEG), transmission electron microscopy (TEM, Philips, Tecnai G2 F30 S-TWIN, 300 kV), and focused-ion beam spectroscopy (FIB). The crystal structures of the LFP, CLFP, and GLFP were confirmed by X-ray powder diffraction (XRD, Rigaku D/MAX-IIIC, 3 kW). The residual carbon content, Brunauer-Emmett-Teller (BET) specific surface area and pore volume/size analysis, and tap density of each sample were measured by the same method as described previously.[4]

**2.2. Cell Fabrication and Electrochemical Analysis.** The fabrication method of electrodes was conducted similarly as described previously.[4] The electrodes were prepared by coating slurries consisting of each active material (75 wt %) with acetylene carbon black (17 wt %) and poly(vinylidene fluoride) (PVdF) (8 wt %) as a binder dissolved in *N*-methyl-2-pyrrolidene (NMP) solution on an Al foil substrate and then dried at 120 °C for 6 h in a vacuum oven. The Li/LFP cells were assembled in a 2016 coin-type cell configuration in an argon-filled glove box. A polypropylene separator soaked with a liquid electrolyte of 1 M $LiPF_6$ dissolved in a 1:1 volume ratio of ethylene carbonate (EC) and dimethyl carbonate (DMC) was placed between the electrode and the Li metal foil (Cyprus Foote Mineral, 99.98%, USA) in the cell.

The charge/discharge characteristics of the fabricated cells were measured with a battery cycler (WBCS3000, Won-A Tech). For the initial cycle, the cells were charged at a constant current density of 0.1 C-rate until 4.3 V (vs. $Li^+/Li$), were continuously applied at a constant voltage of 4.3 V until a capacity of 0.05 C-rate, and then discharged at a constant current density of 0.1 C-rate until 2.0 V. From the 2$^{nd}$ cycle onward, the cells were charged and discharged (0.1 C-rate) galvanostatically between 2.0 and 4.3 V. Finally, the electrode resistances of the materials were estimated from their galvanostatic intermittent titration technique (GITT) results obtained in the voltage range of 2.0−4.3 V.

## 3. RESULTS AND DISCUSSION

To fabricate the graphene embedded $LiFePO_4$ (GLFP), at first, the graphene oxide was synthesized from natural graphite flakes

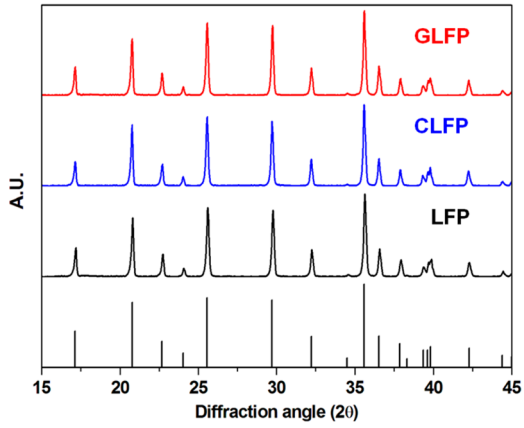


**Figure 2.** XRD patterns of the pristine $LiFePO_4$ (LFP), carbon coated $LiFePO_4$ (CLFP), and graphene embedded $LiFePO_4$ (GLFP).

by a modified Hummer's method, and the pristine $LiFePO_4$ (LFP) (~500 nm) was synthesized by the hydrothermal process. The obtained LFP was further dispersed into ethanol, and then APTMS was poured into the solution. Then, the solution was refluxed for 2 h under argon atmosphere to attach amine groups ($-NH_2$) on the surface of LFP. The formation of the amine groups ($-NH_2$) on the surface of LFP was confirmed by the zeta potential measurements of the LFP and APTMS-modified LFP, as shown in Figure S1, Supporting Information. It is believed that the modification with APTMS made a positively charged surface due to the amine groups ($-NH_2$) of the APTMS molecular structure. The GLFP was produced by the EDC/NHS coupling reaction between amine groups ($-NH_2$) on LFP and carboxyl groups ($-COOH$) on graphene oxide. In particular, The EDC/NHS catalyst was added into a pH controlled aqueous graphene oxide solution. Then, APTMS-modified LFP suspension was poured into the


dx.doi.org/10.1021/am405335k | ACS Appl. Mater. Interfaces 2014, 6, 4731−4736

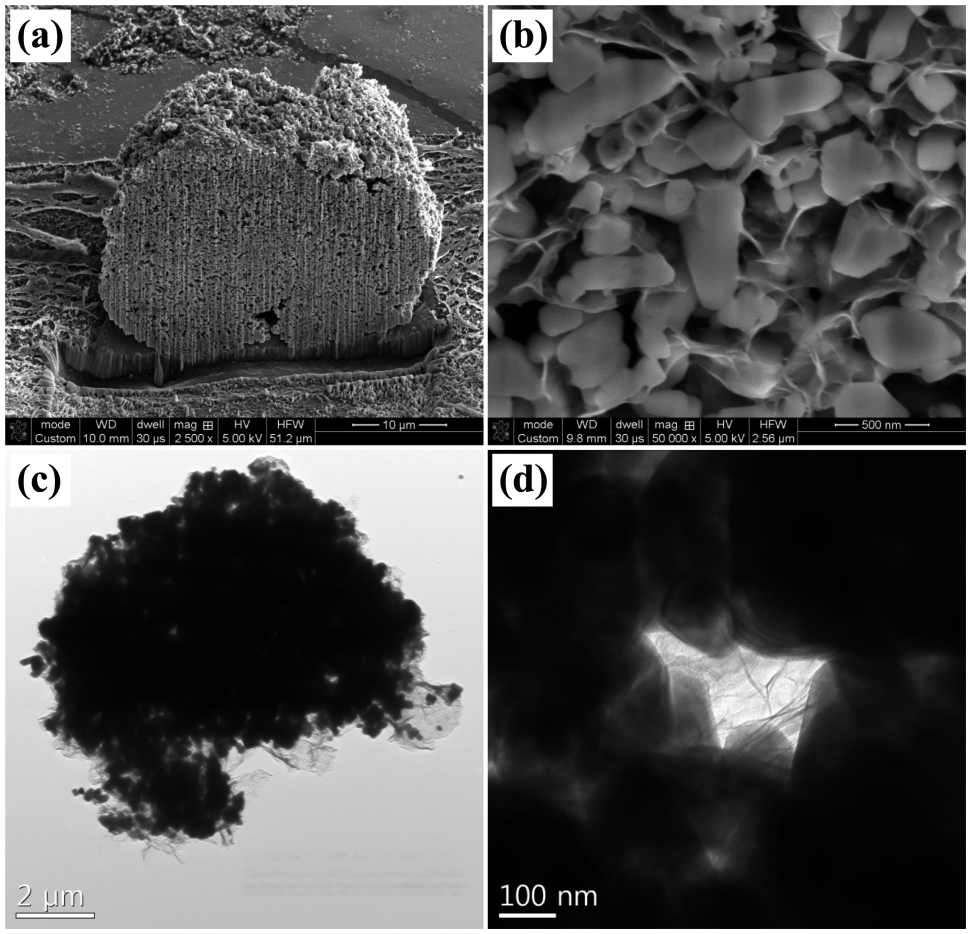


**Figure 3.** (a,b) FIB-SEM and (c,d) TEM images of the graphene embedded $LiFePO_4$ (GLFP).

solution under mild stirring. After 1 h, hydrazine was added into the suspension to reduce graphene oxide to graphene. The process mentioned above is called a "catalyst assisted assembly method", and the schematic illustration was shown in Figure 1. Also, the carbon coated $LiFePO_4$ (CLFP) was made by the sucrose mixing method as a reference for comparison. XRD patterns of the LFP, CLFP, and GLFP shown in Figure 2 demonstrated that the phases of samples were not changed after carbon coating and graphene embedding, and the carbon contents measured by the elemental analyzer were adjusted at ~3 wt % for both CLFP (~3.01 wt %) and GLFP (~2.99 wt %).

The morphology and microstructure of GLFP were examined by scanning electron microscopy (SEM) and transmission electron microscopy (TEM) shown in Figure 3. The GLFP had a round shape with an estimated diameter of ~20 um and was composed of innumerable LFP nanoparticles. The internal morphology and structure of GLFP were examined by focused-ion beam (FIB)-SEM analysis to verify the inner pores of it in Figure 3a,b. From the cross sectional image and their magnified one, many pores existed in the unique structure of GLFP and were distributed uniformly. Furthermore, the existence of graphene sheets embedded in the structure was obviously clarified by the cross sectional images of GLFP. To further examine the extent of incorporation and embedment of graphene sheets in the GLFP, TEM investigations were conducted and the results were shown in Figure 3c,d. Graphene sheets were found at both the surface and core of GLFP. It was verified that the GLFP structure was assembled from LFP nanoparticles with graphene sheets. In addition, many pores were found in the GLFP, providing a porous structure. It is expected that the co-existence of graphene sheets and many pores could provide the conducting path of electrons and facilitated the Li-ion diffusion into the structure. Additional SEM images of the LFP, CLFP, and GLFP and TEM image of the CLFP are presented in Figures S2 and S3, Supporting Information. The estimated tap density of the CLFP and GLFP are ~0.86 g $cm^{-3}$ and ~1.22 g $cm^{-3}$, respectively, which are higher than that (~0.84 g $cm^{-3}$) of the carbon-free LFP. The relatively high tap density of the GLFP compared with the CLFP might be attributed to the micro-sized and porous GLFP with 3D-assembled structure of LFP primary nanoparticles and graphene sheets, as shown in Figure 3.

Figure 4a shows the Fourier transform infrared (FT-IR) spectrum of the LFP and GLFP samples in the wavenumber range of 500−2000 $cm^{-1}$. The local binding types of materials can be investigated by FT-IR analysis. The intensive bands for the spectrum of the LFP and GLFP were strong absorptions at ~950 and ~1050 $cm^{-1}$, commonly. These absorption were attributed to the symmetric stretching vibration mode of O−P−O in tetraphosphate compounds. However, the two samples exhibited a different aspect at around 1600 $cm^{-1}$ shown in the inset of Figure 4a. While LFP had no remarkable bands, GLFP had a band at ~1580 $cm^{-1}$ assigned to the stretching vibration mode of C−C included in graphene. In addition, two bands at

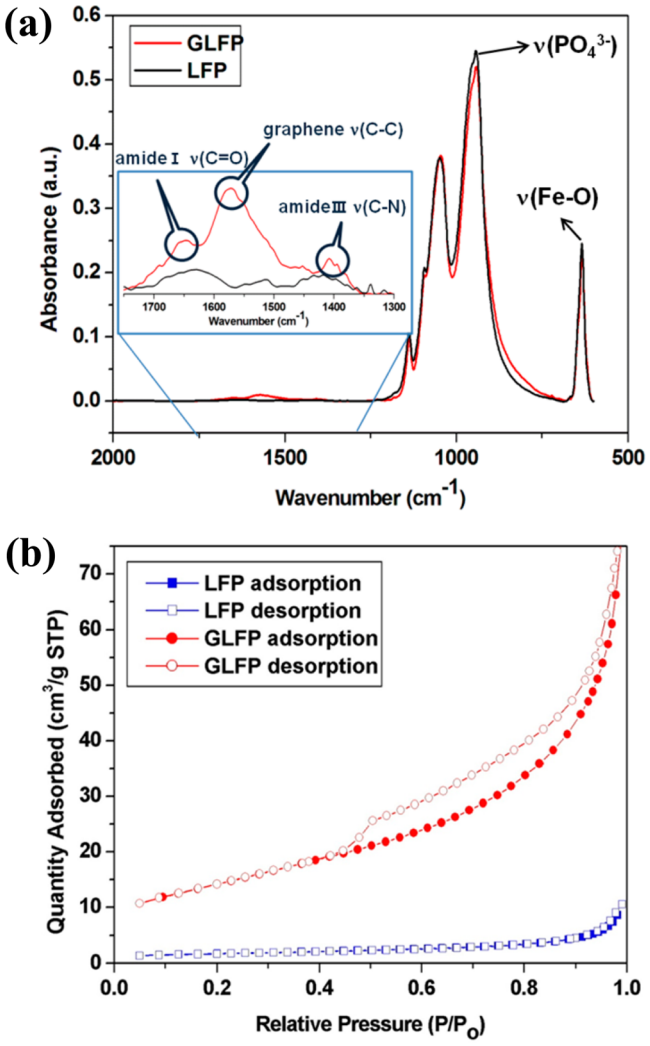


**Figure 4.** (a) FT-IR spectrum and (b) $N_2$ adsorption−desorption isotherms analysis of the pristine $LiFePO_4$ (LFP) and graphene embedded $LiFePO_4$ (GLFP).

**Table 1. BET Specific Surface Area, Pore Volume, and Pore Size of the Pristine $LiFePO_4$ (LFP) and Graphene Embedded $LiFePO_4$ (GLFP)**

| | BET specific surface area ($m^2\ g^{-1}$) | pore volume ($cm^3\ g^{-1}$) | pore size (nm) |
|---|---|---|---|
| LFP | 6.319 | 0.016 | 9.304 |
| GLFP | 50.876 | 0.118 | 10.332 |

~1650 and ~1400 $cm^{-1}$ corresponded to an amide 1 band of the stretching vibration (C═O) and an amide 3 band of the stretching vibration (C−N), respectively. From the spectrum of FT-IR, it was confirmed that the stable amide bonds were formed between LFP and graphene, and the unique structure of GLFP was attributed to this bond. In order to verify the pores in the LFP and GLFP, the nitrogen adsorption−desorption isotherms of samples were performed and shown in Figure 4b. Each sample shows obviously different isotherms confirming the existence of pores. For the LFP, the isotherm is similar to a type II (IUPAC classification) indicating non-porous material. On the other hand, in the case of GLFP, the isotherm shows obviously a type IV (IUPAC classification) with some type II contribution, a kind of mesoporous material. The hysteresis

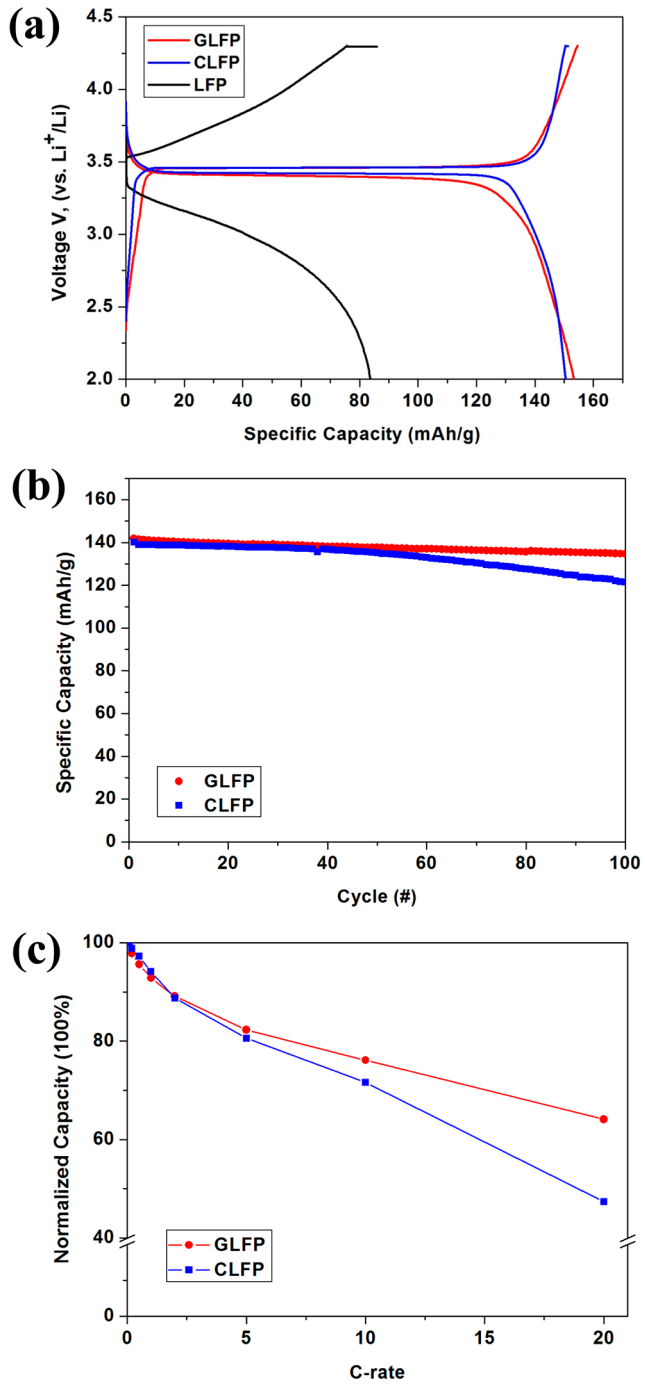


**Figure 5.** (a) Initial galvanostatic voltage profiles of the pristine $LiFePO_4$ (LFP), carbon coated $LiFePO_4$ (CLFP), and graphene embedded $LiFePO_4$ (GLFP) at 0.1 C-rate. (b) Cycling performance of the CLFP and GLFP at 1 C-rate. (c) Normalized rate-capabilities of the CLFP and GLFP.

loop was found in the relative pressure range of 0.5−1.0. The result indicates that the porous structure of GLFP is related to the large surface area and hence can efficiently provide an innumerable reaction site with Li-ion. The large surface area and pore of GLFP were verified by the surface area analysis, as shown in Table 1. The BET specific surface area and pore volume of GLFP were improved about 8 times compared with those of LFP.

The LFP, CLFP, and GLFP were tested as a cathode material for LIBs. Figure 5a shows the initial galvanostatic voltage


dx.doi.org/10.1021/am405335k | ACS Appl. Mater. Interfaces 2014, 6, 4731−4736

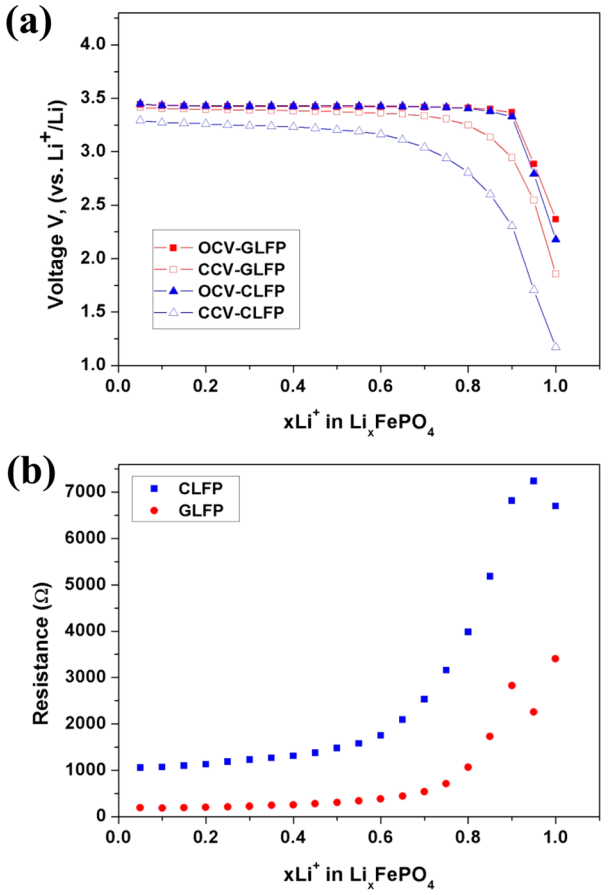


**Figure 6.** (a) Transient voltage profile of the carbon coated $LiFePO_4$ (CLFP) and graphene embedded $LiFePO_4$ (GLFP) by GITT and its OCV/CCV transient curves upon initial discharge. (b) Electrode resistance of the CLFP and GLFP by the potential difference between OCV and CCV.

profiles for the LFP, CLFP, and GLFP at 0.1 C-rate. Though the LFP has nanoscale particles, its discharge capacity is ~85 mA h $g^{-1}$, which is much lower than the theoretical discharge capacity of LFP because the electrical connection between the nanoscale LFP particles is not complete due to the deficiency of conducting carbons. In contrast, the CLFP and GLFP exhibited high discharge capacities of ~150 and ~153 mA h $g^{-1}$, respectively. Figure 5b shows the cycling performance of the CLFP and GLFP at 1 C-rate. After 100 cycles, the GLFP exhibited a high discharge capacity of 135 mA h $g^{-1}$, corresponding to 95.0% of its initial discharge capacity, whereas the CLFP showed a discharge capacity of 121 mA h $g^{-1}$, 86.7% of its initial discharge capacity. The normalized rate-capabilities of the CLFP (150 mA h $g^{-1}$ = 100%) and GLFP (153 mA h $g^{-1}$ = 100%) are represented in Figure 5c. There was no significant difference between CLFP and GLFP at relatively low current density (<2 C-rate). However, the discharge capacity of the CLFP was decreased abruptly at relatively high current density (>5 C-rate). Therefore, the GLFP presented the rate-capability better than the CLFP. The discharge capacity of the GLFP (98.1 mA h $g^{-1}$ = 64.1%) was much higher than that of the CLFP (71.1 mA h $g^{-1}$ = 47.4%) at the high current density of 20 C-rate. These better electrochemical performances of GLFP than that of CLFP are attributed to the use of superior conductive graphene and also to the particle morphology of the GLFP characterized by the large reaction area due to its porous structure.

Figure 6a presents the transient voltage profile of the CLFP and GLFP obtained from the galvanostatic intermittent titration technique (GITT) and its open circuit voltage (OCV)/closed circuit voltage (CCV) transient curves upon initial discharge. It has been reported that an electrode resistance is correlated with the polarization ($\Delta V$) by ohm's law ($R = \Delta V/I$). Thus, the electrode resistance can be estimated from the potential difference between OCV and CCV, as shown in Figure 6b. During the initial discharge, the overall electrode resistance of the GLFP through the whole depth of the discharge was calculated to be much lower (>1000 Ω) than that of the CLFP, suggesting that Li-ion could be more readily inserted into the structure of the GLFP compared with that of CLFP.

## 4. CONCLUSIONS

In conclusion, porous and coarse (~20 μm) graphene embedded $LiFePO_4$ was successfully fabricated by the catalyst assisted assembly method. The unique porous and coarse structure consisting of $LiFePO_4$ nanoparticles and graphene sheets was clarified by TEM, FIB-SEM, and $N_2$ adsorption–desorption analysis. The stable amide bonds between $LiFePO_4$ and graphene were formed by the EDC-NHS coupling reaction used as catalyst. The superior cycling performance and rate-capability of the graphene embedded $LiFePO_4$ compared with that of carbon coated $LiFePO_4$ is attributed to the use of an excellent conductive graphene framework, and a large reaction area resulted from the innumerable pore tunnels formed inside the graphene embedded $LiFePO_4$. This assembly method can be widely used as another promising cathode material for LIBs.

## ■ ASSOCIATED CONTENT

### Supporting Information

Additional materials characterization (zeta potentials, SEM and TEM images). This material is available free of charge via the Internet at http://pubs.acs.org.

## ■ AUTHOR INFORMATION

### Corresponding Authors

*Tel: +82-41-559-3355. Fax: +82-41-559-3158. E-mail: jyeom@katech.re.kr (JiYong Eom).

*Tel: +82-42-350-3326. Fax: +82-42-350-3310. E-mail: hskwon@kaist.ac.kr (HyukSang Kwon).

### Notes

The authors declare no competing financial interest.

## ■ ACKNOWLEDGMENTS

This work was supported by the Center for Inorganic Photovoltaic Materials (No. 2012-0001167) grant funded by the Korea government (MSIP).

## ■ REFERENCES

(1) Padhi, A. K.; Nanjundaswamy, K. S.; Goodenough, J. B. *J. Electrochem. Soc.* **1997**, *144*, 1188–1194.

(2) Wang, Y.; He, P.; Zhou, H. *Energy Environ. Sci.* **2011**, *4*, 805–817.

(3) Yuan, L. X.; Wang, Z. H.; Zhang, W. X.; Hu, X. L.; Chen, J. T.; Huang, Y. H.; Goodenough, J. B. *Energy Environ. Sci.* **2011**, *4*, 269–284.

(4) Han, D. W.; Ryu, W. H.; Kim, W. K.; Lim, S. J.; Kim, Y. I.; Eom, J. Y.; Kwon, H. S. *ACS Appl. Mater. Interfaces* **2013**, *5*, 1342–1347.

(5) Chung, S. Y.; Chiang, Y. M. *Electrochem. Solid-State Lett.* **2003**, *6*, A278−A281.
(6) Prosini, P. P.; Carewska, M.; Scaccia, S.; Wisniewski, P.; Pasquali, M. *Electrochim. Acta* **2003**, *48*, 4205−4211.
(7) Kavan, L.; Exnar, I.; Cech, J.; Graetzel, M. *Chem. Mater.* **2007**, *19*, 4716−4721.
(8) Muraliganth, T.; Murugan, A. V.; Manthiram, A. *J. Mater. Chem.* **2008**, *18*, 5661−5668.
(9) Ding, Y.; Jiang, Y.; Xu, F.; Yin, J.; Ren, H.; Zhuo, Q.; Long, Z.; Zhang, P. *Electrochem. Commun.* **2010**, *12*, 10−13.
(10) Wang, H.; Yang, Y.; Liang, Y.; Cui, L.; Casalongue, H. S.; Li, Y.; Hong, G.; Cui, Y.; Dai, H. *Angew. Chem., Int. Ed.* **2011**, *50*, 1−6.
(11) Wang, Y.; Feng, Z. S.; Chen, J. J.; Zhang, C. *Mater. Lett.* **2012**, *71*, 54−56.
(12) Zhu, Y.; Murali, S.; Cai, W.; Li, X.; Suk, J. W.; Potts, J. R.; Ruoff, R. S. *Adv. Mater.* **2010**, *22*, 3906−3924.
(13) Lee, J. K.; Smith, K. B.; Hayner, C. M.; Kung, H. H. *Chem. Commun.* **2010**, *46*, 2025−2027.
(14) Zhou, X.; Wang, F.; Zhu, Y.; Liu, Z. *J. Mater. Chem.* **2011**, *21*, 3353−3358.
(15) Paek, S. M.; Yoo, E. J.; Honma, I. *Nano Lett.* **2009**, *9*, 72−75.
(16) Wang, H.; Cui, L. F.; Yang, Y.; Casalongue, H. S.; Robinson, J. T.; Liang, Y.; Cui, Y.; Dai, H. *J. Am. Chem. Soc.* **2010**, *132*, 13978−13980.
(17) Yang, S.; Feng, X.; Ivanovici, S.; Mullen, K. *Angew. Chem., Int. Ed.* **2010**, *49*, 8408−8411.
(18) Tang, Y.; Huang, F.; Bi, H.; Liu, Z.; Wan, D. *J. Power Sources* **2012**, *203*, 130−134.
(19) Ha, J. H.; Park, S. K.; Yu, S. H.; Jin, A.; Jang, B. C.; Bong, S. Y.; Kim, I.; Sung, Y. E.; Piao, Y. *Nanoscale* **2013**, *5*, 8647−8655.
(20) Whittingham, M. S. *Dalton Trans.* **2008**, 5424−5431.
(21) Bruce, P. G.; Scrosati, B.; Tarascon, J.-M. *Angew. Chem., Int. Ed.* **2008**, *47*, 2930−2946.